Renewable Energy 147 (2020) 2345–2357

Contents lists available at ScienceDirect

Renewable Energy

journal homepage: www.elsevier.com/locate/renene

Thermohydraulic performance enhancement of a new hybrid duct solar air heater with inclined rib roughness

C. Sivakandhan [a], T.V. Arjunan [b, *], M.M. Matheswaran [c]

[a] Department of Mechanical Engineering, Sri Indu Institute of Engineering and Technology, Sheriguda, Hyderabad, 501510, India
[b] Department of Mechanical Engineering, Coimbatore Institute of Engineering and Technology, Coimbatore, Tamilnadu, 641109, India
[c] Department of Mechanical Engineering, Jansons Institute of Technology, Coimbatore, Tamilnadu, 641659, India

ARTICLE INFO

Article history:
Received 7 March 2019
Received in revised form
2 October 2019
Accepted 3 October 2019
Available online 10 October 2019

Keywords:
Hybrid duct
Inclined ribs
Thermal efficiency
Effective efficiency
Solar air heater

ABSTRACT

In this work, a new hybrid duct configuration of solar air heater is analytically investigated to improve the thermal performance of the system. The proposed design consists of parallel pass air flow paths with rectangular and triangular cross sections at upper and lower sides of the absorber plate. Both the sides of the absorber plates are roughened with inclined shape ribs. The roughness parameters are configured with relative roughness pitch at the bottom of the plate (P_b/e_b) of 4–16, relative roughness height of e/D_h ranges from 0.021 to 0.050 and relative angle of arc of ($\alpha/60$) 0.5–1. Based on the analytical results it is concluded that the maximum effective efficiency is 80.1% for roughness pitch of 8, relative roughness height of 0.021 and relative angle of arc of ($\alpha/60$) 0.5, at the mass flow rate of 0.045 kg/s at the upper and lower duct. The effect of the mass flow fraction (i) on the thermal performance of the solar air heater is also analyzed. The system improves the thermal and effective efficiency by 22.4% and 18.1% when compared to conventional rectangular duct parallel pass SAH. The design plots are developed to find the optimum values of roughness parameters with respect to ambient conditions.

1. Introduction

Among the available solar thermal energy conversion devices, solar air heaters are simple in design, widely used and require lesser maintenance. Due to its own merits it is used for the applications like space heating, drying of industrial and agricultural products. And also, it is used to improve the performance of desalination system and heat pumps. Even though it contains its usefulness still the thermal performance of the solar air heater (SAH) is poor due to its adverse effect of thermo physical properties of air, which leads to decrease the convective heat transfer coefficient between the absorber plate and moving air. Various researchers reported different methodologies to overcome the drawback and to improve the efficiency. One of the effective technique is by flowing air on both the side of the absorber plate which increases the surface area and the rate of heat transfer [1]. Yeh et al. [2] develops an analytical model and experimental work to evaluate the performance of parallel pass double duct SAH (PPDDSAH). From the analysis, it is concluded the system is more efficient than the device with a single flow path.

El-sebaii et al. [3,4] compares the thermo hydraulic performance of PPDDSAH with PPDDSAH attached with v-corrugated plates and PPDDSAH with fins. They reported that there is an improvement in performance about 11–14% with former and 9.3–11.9% with later. Dhaiman et al. [5] carried out the analytical and experimental performance analysis of parallel flow packed bed SAH and study the effects of bed porosity at the upper duct on the thermal performance. The system improves the performance about 10–20% when compared with PPDDSAH. Further comparison is carried out between the parallel flow packed bed SAH with counter flow packed bed SAH and it is reported that parallel flow SAH is more efficient at higher flow rates [6]. The thermo hydraulic performance of parallel pass jet impingement solar air heater is investigated analytically and the result shows that the jet diameter has a higher influence on the thermal performance of SAH. Further, it improves the effective efficiency by 21.2% [7,8]. From the ref. [1–8] it is known that parallel pass SAH are effectively improving the performance at higher flow rates.

On the other hand, researchers are also used artificial roughness on the absorber plate for improving the effective efficiency. The

* Corresponding author.
E-mail addresses: kandhansiva69@gmail.com (C. Sivakandhan), arjun_nivi@yahoo.com (T.V. Arjunan), madhume01@gmail.com (M.M. Matheswaran).

https://doi.org/10.1016/j.renene.2019.10.007
0960-1481/

Nomenclature

Ap	Absorber plate area (m^2)
C_p	Specific heat of air (J/kgK)
D_h	Hydraulic diameter of air flow channel (m)
e	Relative roughness height
e/Dh	Relative roughness height ratio
e^+	roughness Reynolds number $= e/D_h(\sqrt{f/2})(\mathrm{Re})$
f	Friction factor of duct
g	Acceleration due to gravity (m^2/s)
G	Total mass flow rate (kg/s) $=(m_u + m_l)$
h_c	heat transfer co efficient occurs due to convection (W/m^2K)
h_r	heat transfer co efficient occurs due to Radiation (W/m^2 K)
h_w	heat transfer coefficient happens due to wind, (W/m^2K)
$h_{gu\text{-}gl}$	Free convective heat transfer co efficient between upper and lower glass cover (W/m^2K)
L	Length of the solar air heater duct (m)
m	Mass flow rate of air (kg/s)
Nu	Nusselt number
P_m	Pumping Power (W)
Q_U	Useful heat gain (W)
Re_a	Reynolds Number inside the duct
I	Solar radiation (W/m^2)
i	Mass flow fraction
T	Temperature (K)
U_b	Bottom loss coefficient (W/m^2K)
V_w	Wind Velocity (m/s)
W	Width of the collector (m)
Z_2	Height of the rectangular duct (m)
Z_3	Distance between the glass covers
τ	Transmissivity of glass cover
μ_a	Viscosity (kg/ms)
P_b/e_b	Relative roughness pitch at bottom of absorber plate
ΔP	Pressure drop at air flow channel (N/m^2)
α	Absorptivity
k	Thermal conductivity (W/mK)
ϕ	Tilt angle (°)
ρ_a	Density of air (kg/m^3)
σ	Stefan's Boltzmann constant (W/m^2K^4)
η_I	Thermal Efficiency (%)
η_{eff}	Effective (or) Thermo hydraulic Efficiency
$\alpha/60^0$	Relative angle of arc

Subscripts

am	Ambient air
b	Back plate
gu	Upper glass cover
gl	Lower glass cover
in	Insulation
a	Air in the channel
ao	outlet
p	Absorber plate
sky	Sky
1	Upper flow path (or) back plate number
2	Lower flow path (or) back plate number
l	Lower
u	Upper
i	inlet

presence of roughness breaking the laminar sub layer formulation at turbulent flow regions. It also separates the flow into primary and secondary flow regions, during at reattachment points the boundary layer thickness are nullified and increases the rate of heat transfer [9]. Gupta et al. [10] investigate the thermo hydraulic performance of inclined rib roughed SAH and optimize the roughness dimensions. The thermal performance of V-down discrete ribs SAH is analyzed analytically and the system improves the performance up to the mass flow rate per unit area of the collector is equal to 0.045kg/sm^2 [11]. The enhancement is ranges from 12.5 to 20% when compared with conventional parallel pass SAH [12]. Gawande et al. [13] suggested the angled square ribs for SAH and found that the inclination angle of 20° provides better performance. Bhushan et al. [14] uses protruded roughness geometry and suggested the design plots for finding the maximum effective efficiency of the SAH for obtaining the desired temperature rise values. The analytical investigation for analyzing the arc shape rib roughened SAH by Sahu et al. [15] by varying the height to the hydraulic diameter ratio and flow angle of attack. The results also compared with other roughness designs and optimum operating conditions are reported. Thakur et al. [16] numerically analyze the hyperbolic rib geometry and compare the results with rectangular, triangular and semicircular ribs. The optimum conditions are identified at the Re of 6000, roughness height of 1 mm and roughness pitch of 10 mm. Kumar et al. [17] carried out the experimental investigation on three-sided dimple roughened SAH at actual ambient condition. The influences of roughness parameter on heat transfer and pressure drop are formulated in terms of Nusselt number and friction factor correlation. The Nusselt number improves 3.94 times and friction factor raises about 2.56 times when compared with single side roughed SAH. Kumar and Layek [18] carried out the experimental analysis at indoor working conditions of SAH with twisted tape ribs to evaluate the roughness parameters on the enhancement of heat transfer. The enhancement in heat transfer is measured in terms of thermohydraulic performance is 2.13 times superior than conventional SAH [19]. SAH with square wave profiled transverse ribs is analyzed in ANSYS FLUENT15.0 for the relative roughness pitch of 4–30, Reynolds number of 3000–15000 and for fixed roughness height ratio 0.043. The results show that the thermohydraulic performance is 1.43 for the relative roughness pitch of 10 and, Reynolds number of 12000 [20]. A new V rib roughness design is proposed by the Jain et al. [21] and concluded that the placement of staggered rib in front of the opening enhances the heat transfer and friction factor. Gabhane et al. [22] carried out experimental analysis on PPSAH attached with c type roughness and also the statistical correlation is developed to predict the Nusselt number and friction factor with 12% of accuracy.

From the ref. [8–22] it is concluded that using of artificial roughness improves the heat transfer and friction factor. The increment in friction factor, increases the pumping power consumption and decreases the thermohydraulic performance at desired flow rates. To overcome these limitations, researchers are developing triangular duct solar air heater. Triangular cross-sectional duct offers less friction factor when compared with any other cross-sectional ducts [23]. The effect of apex angle and dimple roughness parameter on the performance of triangular duct SAH had reported by Goel [24]. It is concluded that at the apex angle of 60° the dimple roughened SAH performs better. Further the dimple, and circular shape rib roughened absorber plates are

attached to a smooth curve triangular duct SAH had analyzed that enhances the heat transfer by a maximum of 110% [25,26]. Kumar et al. [27] had carried out the experimental and numerical study on dimple roughened SAH and reported the influence of smooth curves on all three corners. The smooth curve increases the velocity at the centre of the duct, which enhances the heat transfer. The CFD analysis is carried out for triangular duct solar air heaters which are combined with circular, square and chamfered rib roughness and enhances the performance about 1.99,1.97 and 1.19 times respectively when compared with conventional SAH [28–30]. Bharadwaj et al. [31] had experimentally carried out the performance of inclined rib roughened triangular duct SAH and identify the optimum design conditions of relative roughness pitch of 12, relative roughness height of 0.043 and angle of attack of 60°.

From the above literature, it is concluded that SAH performances are improved by using a parallel pass flow arrangement, using artificial roughness and by modifying the cross section of the duct into triangular shape. As per the author's knowledge, no work is attempting to combine all these techniques to improve the performance. Therefore, in this work all these three methods are integrated and proposed a new configuration SAH is called parallel pass hybrid duct solar air heater. In the proposed model consist of upper air flow path with rectangular and lower air flow path with triangular cross section. Further improving the efficiency, the inclined shape rib roughness are attached at the top and bottom of the absorber plate. The objectives of the present work are: (I) To evaluate the thermal and thermo hydraulic performance of the proposed configuration of the solar air heater by developing a mathematical model. (ii) To optimize the rib roughness parameters as an effective pitch ratio at the bottom of the absorber plate (P_b/e_b), effective height ratio (e/D_h), the effective angle of arc ($\alpha/60$) and mass flow fraction (i) for yielding maximum effective efficiency. (iii) Then suggesting the design plots to identify the rib roughness parameters which yields the maximum effective efficiency for obtaining the desired temperature rise.

2. Mathematical modeling

The schematic layout of parallel pass hybrid duct solar air heater with inclined ribs is shown in Fig. 1 a. It consist of two air flow paths on upper and lower sides of the absorber plate. The lower glass cover is attached at Z_2 distance from the top side of artificially roughened absorber plate. This formulates the upper flow air flow path with rectangular cross section. The triangular cross-sectional lower air flow path is made up of two back plates and lower surface of the absorber plate. The upper glass cover is attached over the lower glass cover at a distance of Z_3 for minimizing the top heat loss. The side and bottom plates are well insulated to reduce the heat loss to the ambient. Fig. 1 c. Shows the design details of inclined shape artificial rib roughness parameters. By considering the subsequent assumptions the energy balance equation for each component of SAH is developed [32].

I. The mathematical model is developed and analyzed under steady state operating conditions
II. The temperature variation happens only along the length of the air heater is considered and on other two dimensions are negligible.
III. The energy stored in solar air heater components (upper and lower glass cover, Roughened absorber plate, inclined back plates and insulation) is negligible.
IV. For all the wavelength of radiation, sky is assumed as black body and its temperature is equal to the ambient temperature.
V. It is assumed that the upper and lower ducts are completely free from air leakage.

2.1. Energy balance for upper glass cover

The basic parameters which are required to formulate the mathematical model are shown in Fig. 1 b. Eqn. (1) expresses the energy balance happens at top glass cover. The left-hand side terms of the equation show the energy input to the upper glass cover from solar insolation and lower glass cover through convection and radiation mode of heat transfer. The right-hand side terms, express that energy loss from the glass cover.

$$\alpha_{gu}S + h_{r,\,gl-gu}\left(T_{gl}-T_{gu}\right) + h_{c,\,gl-gu}\left(T_{gl}-T_{gu}\right) = h_w\left(T_{gu} - T_{am}\right) + h_{r,\,g-s}\left(T_{gu}-T_{sky}\right) \quad (1)$$

2.2. Energy balance for lower glass cover

The lower glass cover receives energy from top surface of the absorber plate and solar radiation passed through the upper glass cover. Then the part of energy released with the top glass cover and the remaining energy is taken by flowing air at the upper duct. This energy transfer phenomena are as stated

$$\alpha_{gl}\tau_{gu}S + h_{r,p-gl}\left(T_p-T_{g1}\right) = h_{r,gl-gu}\left(T_{gl}-T_{gu}\right) + h_{c,gl-gu}\left(T_{gl} - T_{gu}\right) + h_{c,gl-a1}\left(T_{gl}-T_{a1}\right) \quad (2)$$

Energy balance in the air flowing at upper duct.

The air flowing at upper rectangular duct receives energy from artificially roughened absorber plate and lower glass cover. The energy balance equation for flowing air can be written as

$$h_{c,\,p-a1}\left(T_p - T_{a1}\right) + h_{c,\,gl-a1}\left(T_{gl}-T_{a1}\right) = q_{u1} \quad (3)$$

In the eqn. (3) $T_{a1} = (T_{a1i}+T_{a1o})/2$ and $q_{u1} = 2\dot{m}_u C_p(T_{a1}-T_{a1i})/A_p$ exemplifies the mean air temperature and worthwhile energy gain at upper rectangular air flow path.

2.3. Energy balance for absorber plate

The artificially roughened collector plate obtains energy from direct solar radiation, which is passed through upper and lower glass cover. The received energy then distributed to flowing air at upper and lower ducts, and other components of the solar air heater. This energy transfer phenomena can be stated as

$$\alpha_p\tau_{gl}\tau_{gu}S = h_{r,p-gl}\left(T_p - T_{gl}\right) + h_{r,p-b1}\left(T_p-T_{b1}\right) + h_{r,p-b2}\left(T_p-T_{b2}\right) + h_{c,p-a1}(T_p-T_{a1}) + h_{c,p-a2}(T_p-T_{a2}) \quad (4)$$

2.4. Energy balance in the air flowing at lower duct

The air flowing at lower triangular duct receives heat from absorber plate and another two back plates. The energy balance equation for flowing air can be written as

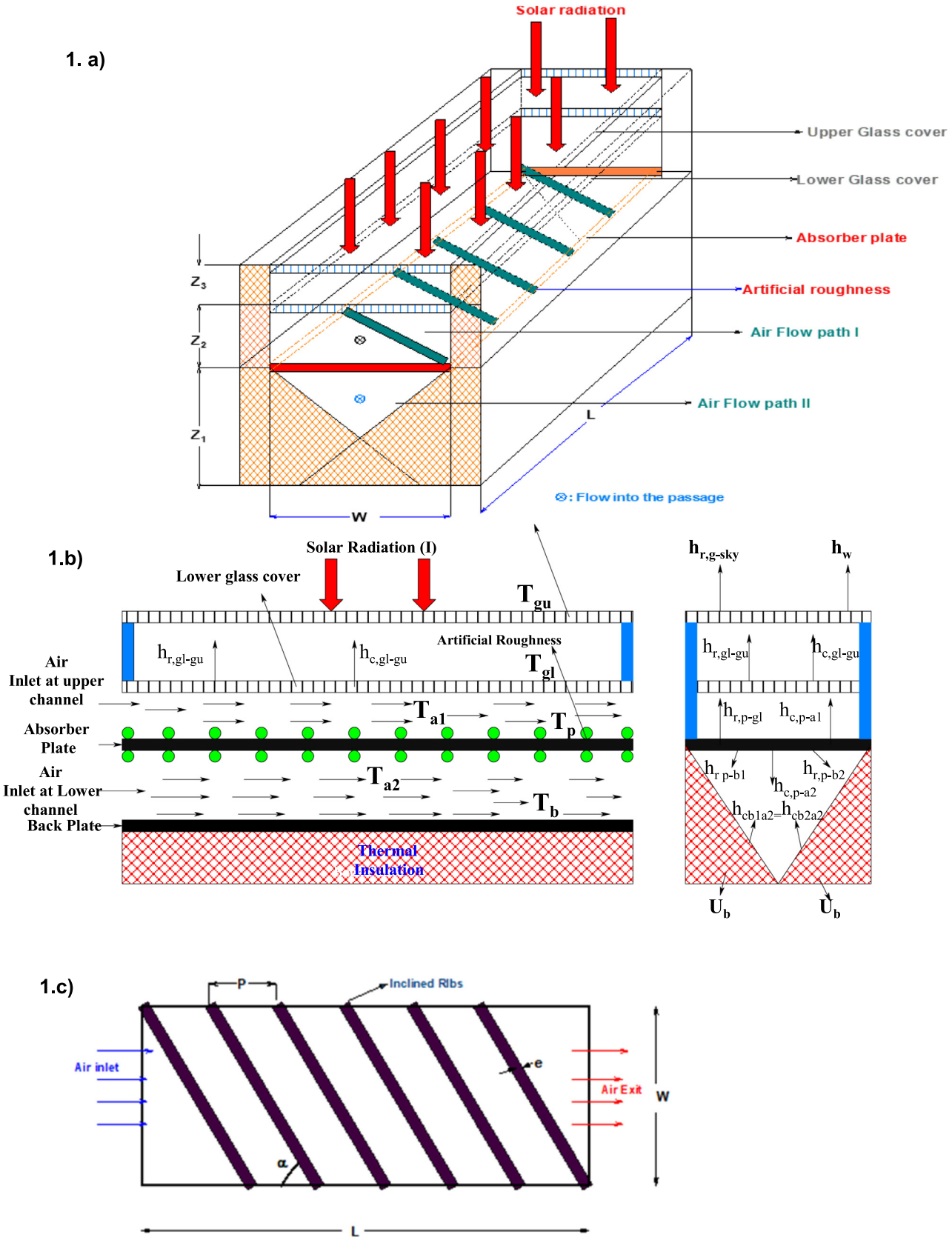

Fig. 1. (**a**) Schematic lay out of PPHDSAH (**b**) Energy balance for PPHDSAH (**c**) Roughness parameters with absorber plate.

$$h_{c,\ p-a2}(T_p - T_{a2}) + h_{c,\ b1-a2}(T_{b1} - T_{a2}) + h_{c,\ b2-a2}(T_{b2} - T_{a2}) = q_{u2} \quad (5)$$

In the eqn. (5) $T_{a2} = (T_{a2i} + T_{a2o})/2$ and $q_{u2} = 2\dot{m}_l C_p (T_{a2} - T_{a2i})/A_p$ exemplifies the mean air temperature and worthwhile energy gain at lower triangular air flow path.

2.5. Energy balance for back plates

The lower triangular duct consists of two back plates which receive energy from absorber plate and transfer the energy to the air flowing at lower duct. The remaining heat is lost to the ambient due to the temperature difference. It can be stated as follows.

For back plate: 1

$$h_{r,p-b1}\left(T_p - T_{b1}\right) = h_{c,\ b1-a2}\left(T_{b1} - T_{a2}\right) + U_b(T_{b1} - T_{am}) \quad (6)$$

For back plate: 2

$$h_{r,p-b2}\left(T_p - T_{b2}\right) = h_{c,\ b2-a2}\left(T_{b2} - T_{a2}\right) + U_b(T_{b2} - T_{am}) \quad (7)$$

2.6. Determination of temperature of various solar air heater components

To determine the temperature of solar air heater components the Eqns. (1)–(7) are rearranged as follows

$$T_{gu} = \frac{\alpha_{gu} S + \left(h_{r,\ gl-gu} + h_{c,\ gl-gu}\right) T_{gl} + h_w T_{am} + h_{r,\ gu-sky} T_{sky}}{\left(h_w + h_{r,\ gu-sky} + h_{r,\ gl-gu} + h_{c,\ gl-gu}\right)} \quad (8)$$

$$T_{gl} = \frac{\tau_{gu}\alpha_{gl} S + \left(h_{r,\ gl-gu} + h_{c,\ gl-gu}\right) T_{gu} + h_{c,gl-a1} T_{a1} + h_{r,p-gl} T_p}{\left(h_{r,p-gl} + h_{c,gl-a1} + h_{r,\ gl-gu} + h_{c,\ gl-gu}\right)} \quad (9)$$

$$T_{a1} = \frac{h_{c,gl-a1} T_{g1} + h_{c,p-a1} T_p + \left[\frac{2mc_p}{WL}\right] T_{a1i}}{\left(h_{c,p-a1} + h_{c,gl-a1}\right) + \left[\frac{2mc_p}{WL}\right]} \quad (10)$$

$$T_p = \frac{\tau_{gu}\tau_{gl}\alpha_p S + h_{r,p-gl} T_{gl} + h_{c,p-a1} T_{a1} + h_{c,p-a2} T_{a2} + h_{r,p-b1} T_{b1} + h_{r,p-b2} T_{b2}}{\left(h_{r,p-gl} + h_{r,p-b1} + h_{r,p-b2} + h_{c,p-a1} + h_{c,p-a2}\right)} \quad (11)$$

$$T_{a2} = \frac{h_{c,p-a2} T_p + h_{c,b1-a2} T_{b1} + h_{c,b2-a2} T_{b2} + \left[\frac{2mc_p}{WL}\right] T_{a2i}}{\left(h_{c,p-a2} + h_{c,b1-a2} + h_{c,b2-a2}\right) + \left[\frac{2mc_p}{WL}\right]} \quad (12)$$

$$T_{b1} = \frac{h_{r,p-b1} T_p + h_{c,b1-a2} T_{a2} + U_{b1} T_{am}}{\left(h_{r,p-b1} + h_{c,b1-a2} + U_{b1}\right)} \quad (13)$$

$$T_{b2} = \frac{h_{r,p-b2} T_p + h_{c,b2-a2} T_{a2} + U_{b2} T_{am}}{\left(h_{r,p-b2} + h_{c,b2-a2} + U_{b2}\right)} \quad (14)$$

2.7. Heat transfer coefficients

The convective heat transfer coefficient occurs between the upper glass cover to the ambient due to blowing air is calculated using the empirical correlation as follows [7].

$$h_w = 2.8 + 3.3 V_w \quad (15)$$

The radiative heat transfer coefficient between the upper glass cover and sky is given by

$$h_{r,\ gu-sky} = \sigma \varepsilon_{gu}\left(T_{gu} + T_{sky}\right)\left(T_{gu}^2 + T_{sky}^2\right) \quad (16)$$

In the eqn. (16) the sky temperature is given by

$$T_{sky} = 0.0552 T_{am}^{1.5} \quad (17)$$

The radiative heat transfer coefficient between the upper and lower glass cover can be calculated using the relationship as follows [33].

$$h_{r,\ gl-gu} = \frac{\sigma\left(T_{gl}^2 + T_{gu}^2\right)\left(T_{gl} + T_{gu}\right)}{\frac{1}{\varepsilon_{gl}} + \frac{1}{\varepsilon_{gu}} - 1} \quad (18)$$

The natural convective heat transfer coefficient occurs between the upper and lower glass cover is calculated as follows [7].

$$h_{c,\ gl-gu} = \frac{k_a}{Z_3} Nu_{c,gl-gu} \quad (19)$$

$$Nu_{c,gl-gu} = 1 + 1.44\left[1 - \frac{1708(\sin 1.8\ \phi)^{1.6}}{Ra\ \cos\phi}\right]\left[1 - \frac{1708}{Ra\ \cos\phi}\right]^{+} + \left[\left(\frac{Ra\ \cos\phi}{5830}\right)^{1/3} - 1\right]^{+} \quad (20)$$

In the eqn. (20) the term ϕ represents a collector tilt angle. The validity of the above correlation ranges from 0° to 60° of the collector tilt angle. The 3rd and 4th term of the above equation is considered only if it yields the positive value. The Rayleigh number (Ra) is calculated by

$$Ra = \frac{g\beta\left(T_{gl} - T_{gu}\right) Z_3}{\alpha\nu} \quad (21)$$

The radiative heat transfer coefficient between the top surface of artificially roughened absorber plate and bottom surface of the lower glass cover can be calculated using the relationship as follows [33].

$$h_{r,\ p-\ gl} = \frac{\sigma\left(T_p^2 + T_{gl}^2\right)\left(T_p + T_{gl}\right)}{\frac{1}{\varepsilon_p} + \frac{1}{\varepsilon_{gl}} - 1} \tag{22}$$

The forced convective heat transfer coefficient occurs between the absorber plate and flowing fluid in the upper rectangular channel is calculated by

$$h_{c,\ p-a1} = \frac{k}{D_{h1}} Nu_{c,p-a1} \tag{23}$$

The Nusselt number ($Nu_{c,\ p\text{-}a1}$) in the above equation is calculated using the following relationships.

When the system operates with smooth plate [34].

$$Nu_{c,p-a2} = 3.1 \times 10^{-3} (\mathrm{Re}_{a2})^{1.0972} \left(\frac{\alpha}{60}\right)^{0.0792} \left(\frac{P_b}{e_b}\right)^{1.0832} \left(\frac{e}{D_{h2}}\right)^{-1.9854} \exp\left[-0.1908\left[\ln\left(\frac{\alpha}{60}\right)\right]^2\right] \exp\left[-0.246\left[\ln\left(\frac{\mathrm{P}}{\mathrm{e}}\right)\right]^2\right] \tag{31}$$

$$Nu_{c,p-a1} = 5.4 + \frac{0.00190\left(\mathrm{Re}_a \mathrm{Pr}\left[\frac{D_{h1}}{L}\right]\right)^{1.71}}{1 + 0.00563\left(\mathrm{Re}_a \mathrm{Pr}\left[\frac{D_{h1}}{L}\right]\right)^{1.17}} \left(< \mathrm{Re}_a 2300\right) \tag{24}$$

$$Nu_{c,p-a1} = 0.116\left(\mathrm{Re}_a^{2/3} - 125\right)\mathrm{Pr}^{1/3} + \left[1 + \left[\frac{D_{h1}}{L}\right]^{\frac{2}{3}}\right]\left[\frac{\mu}{\mu_w}\right]^{0.14} \left(2300 < \mathrm{Re}_a < 6000\right) \tag{25}$$

$$Nu_{c,p-a1} = 0.018\mathrm{Re}_a^{0.8}\mathrm{Pr}^{0.4}\ (\mathrm{Re_a} > 6000) \tag{26}$$

When the system operates with inclined rib artificially roughened plate [10].

For $e^+ < 35$

$$Nu_{c,p-a1} = 2.4 \times 10^{-3} (\mathrm{Re}_{a1})^{1.084} \left(\frac{e}{D_{h1}}\right)^{0.001} \left(\frac{W}{Z_2}\right)^{-0.06} \exp\left[-0.04\left[1 - \left(\frac{\alpha}{60}\right)\right]^2\right] \tag{27}$$

For $e^+ > 35$

$$Nu_{c,p-a1} = 7.1 \times 10^{-3} (\mathrm{Re}_{a1})^{0.88} \left(\frac{e}{D_{h1}}\right)^{-0.24} \left(\frac{W}{Z_2}\right)^{-0.028} \exp\left[-0.475\left[1 - \left(\frac{\alpha}{60}\right)\right]^2\right] \tag{28}$$

In the above equations from 23 to 28 the hydraulic diameter (D_{h1}) of upper rectangular channel having the width of the W and depth of Z_2 can be calculated as

$$D_{h1} = \frac{4WZ_2}{2(W + Z_2)} \tag{29}$$

In the same way that the forced convective heat transfer coefficient occurs between the artificially roughened absorber plate and flowing fluid in the lower triangular channel is calculated by

$$h_{c,\ p-a2} = \frac{k}{D_{h2}} Nu_{c,p-a2} \tag{30}$$

For smooth plate, it is considered that for finding the value of $Nu_{c,\ p\text{-}a2}$ the correlations listed from eqn. (24)–(26) are used.

When the system operates with inclined rib artificially roughened plate [31].

where the hydraulic diameter (D_{h2}) of the lower triangular duct is calculated as

$$D_{h2} = \frac{0.866W}{3} \tag{32}$$

The radiative heat transfer coefficient between the absorber plate and bottom plates can be calculated using the relationship as follows [33].

$$h_{r,\ p-\ b1} = \frac{F_{p-b1}\sigma\left(T_p^2 + T_{b1}^2\right)\left(T_p + T_{b1}\right)}{\frac{1}{\varepsilon_p} + \frac{1}{\varepsilon_{b1}} - 1} \tag{33}$$

$$h_{r,\ p-\ b2} = \frac{F_{p-b2}\sigma\left(T_p^2 + T_{b2}^2\right)\left(T_p + T_{b2}\right)}{\frac{1}{\varepsilon_p} + \frac{1}{\varepsilon_{b2}} - 1} \tag{34}$$

The convective heat transfer coefficient occurs between the back plates and flowing air in the lower triangular duct is calculated by

$$h_{c,\ b1-a2} = \frac{k_a}{D_{h2}} Nu_{c,b1-a2} \tag{35}$$

In the above equation, it is considered that for finding the value of $Nu_{c,\ b1\text{-}a2}$ and $Nu_{c,\ b2\text{-}a2}$ the correlations listed from eqn. (24)–(26) are used.

The back-loss coefficient is calculated as

$$U_{b1} = U_{b2} = \frac{k_{in}}{\delta_{in}} \tag{36}$$

The thermo physical properties of air are linearly varied with the average temperature of the air (T°C). To calculate the properties the following correlations are used [35,37].

Specific heat

$$C_p = 0.000066(T - 27) + 1.0057 \tag{37}$$

Density

$$\rho_a = 0.00359(T - 27) - 1.1774 \tag{38}$$

Thermal Conductivity

$$k_a = 0.0000758(T - 27) + 0.02624 \tag{39}$$

Viscosity

$$\mu_a = [1.983 + 0.00184(T - 27)] \times 10^{-5} \tag{40}$$

2.7.1. Expenditure of mechanical pumping power for PPHDSAH

To propel the air into the solar air heater it consumes pumping power to overwhelm the resistance along the length of solar air heater channel [7].

$$P_m = \frac{(\dot{m}_u + \dot{m}_l) \times (\Delta P_u + \Delta P_l)}{\rho_a} \tag{41}$$

In the above equation the pressure drop occurs at upper rectangular and lower triangular duct are calculated by means of the relationship

$$\Delta P_u = \frac{2 f_u L V_u^2 \rho_a}{D_{h1}} \tag{42}$$

$$\Delta P_l = \frac{2 f_l L V_1^2 \rho_a}{D_{h2}} \tag{43}$$

In the above eqns. (42) and (43) the friction factors occur in the upper and lower ducts are calculated using following relations.

For smooth plate [10].

$$f_u = f_l = 0.079(\mathrm{Re}_a)^{-0.25} \tag{44}$$

For inclined rib roughened absorber plates [10,31].

$$f_l = 11.845(\mathrm{Re}_{a2})^{-0.693}\left(\frac{\alpha}{60}\right)^{0.0418}\left(\frac{P_b}{e_b}\right)^{1.1389}\left(\frac{e}{D_{h2}}\right)^{0.3365}\exp\left[-0.1686\left[\ln\left(\frac{\alpha}{60}\right)\right]^2\right] \exp\left[-0.2644\left[\ln\left(\frac{P}{e}\right)\right]^2\right] \tag{45}$$

2.8. Thermal and effective efficiency of PPHDSAH

2.8.1. Thermal efficiency

The thermal efficiency of the solar air heater is defined as the ratio between the useful heat gained by the flowing air to the total amount energy supplied by solar insolation. As per first law of thermodynamics it is calculated as [36].

$$\eta_I = \frac{Q_u}{A_p \times I} = \frac{\dot{m}_u C_{pa}(T_{o1a} - T_{i1a}) + \dot{m}_1 C_{pa}(T_{o2a} - T_{i2a})}{A_p \times I} \tag{46}$$

2.8.2. Effective efficiency of PPHDSAH

The actual performance of the SAH is to be calculated by considering additional energy consumption for flowing the air against the friction. The existence of artificial roughness at above and below the absorber plate further increases the pumping power. This mechanical pumping power is divided by conversion factor C_r for calculating the actual pumping power consumption. The effective efficiency is calculated by means of the following relationship [8].

$$C_r = \eta_{Th}\eta_{fr}\eta_m\eta_f \tag{47}$$

$$\eta_{eff} = \frac{Q_u - \left[\frac{P_m}{C_j}\right]}{I \times A_p} \tag{48}$$

In the above equation the value of C_r is equal to 0.2.

2.9. Solution procedure for evaluating the temperature and thermal performance of PPHDSAH

The analytical calculations are carried out for evaluating the temperature of solar air heater components and thermal performance of various configurations of the system. The equations from 8 to 14 are solved simultaneously by using the matrix inversion technique. To solve the equations and analyzing the influence of design and operating conditions a suitable computer code is developed in MATLAB [7].

I. During the execution of the code the fixed parameters like L, W, Z_2, Z_3, I, T_{1ai}, m, i, ϕ, α_p, ε_p, σ, α_{gu}, α_{gl}, etc. are initialized.
II. The initial temperature of glass covers, absorber plate, back plates, and air flow paths are assumed that its values are equal to the ambient temperature (T_{am}). Further the properties of the air are evaluated by using the relationship from 37 to 40.
III. Using the initial inputs, the further parameters like Dh_1, D_{h2}, Re, h_w, $h_{r\ gl\text{-}sky}$, $h_{c,\ gl\text{-}gu}$, $h_{r,\ gl\text{-}gu}$, $h_{r,\ gl\text{-}p}$, $h_{c,\ p\text{-}a1}$, $h_{r,\ b1\text{-}p}$, $h_{c,\ p\text{-}a2}$, $h_{r,\ b2\text{-}p}$ are calculated.
IV. These values are substituted in the eqns. (8)–(14) the new temperature values are calculated. Then the new values are compared with, initially assumed values and if the difference is greater than 0.001 °C then the previously assumed values are replaced by new values. Further, if the condition is satisfied the temperature values are finalized and these values are used to find the thermal performance of the solar air heater.

Table 1
Details of design and operating conditions considered for evaluating the performance of PPHDSAH.

Parameters	Base Values
Fixed Dimensions and functional conditions of SAH	
Length of solar air heater duct, L	1.5 m
Width of solar air heater duct, W	0.290 m
Height of the collector, $Z_2 = H$	0.025 m
Distance between the upper and lower glass cover (Z_3),	0.05 m
Insulation thickness, δ_{in}	0.05 m
Thermal conductivity of insulation k_i	0.037 W/mK
Absorber plate - Emissivity, ε_p	0.9
Bottom plate - Emissivity, ε_b	0.9
Glass cover -Emissivity ε_{gc}	0.88
Effective transmittance absorptance product, $\tau\alpha_p$	0.8
Ambient temperature, T_a	300 K
Wind velocity, V_w	1.5 m/s
Relative roughness pitch at top of absorber plate (P_t/e_t)	10
Variable dimensions and functional conditions of SAH	
Mass flow rate (m)	0.01–0.09 kg/s
Relative roughness height at top and bottom of absorber plate (e/D_h)	0.021–0.05
Relative roughness pitch at bottom (P_b/e_b)	4–16
Relative angle of arc at top and bottom of absorber plate ($\alpha/60^0$)	0.5–1
Solar Intensity, (I)	500–1000 W/m^2
Mass flow fraction(i)	0.1–0.9

3. Results and discussion

The thermal performance of parallel pass hybrid duct parallel pass solar air heater is analyzed analytically and the values of roughness parameters are optimized. The material properties, fixed and variable design parameters, and functional conditions of the SAH are revealed in the Table 1. During the performance evaluation the mass flow rate at upper and lower duct are maintained equal ($m_u = m_l$). Then the influence of mass flow fraction (i) on the performance of SAH is analyzed and the detailed outcomes are as follows.

3.1. Validation of theoretical model

To analyze and optimize the proposed system performance and its design configurations, it is very much essential to validate the proposed model and its solution procedure code developed in MATLAB.

Therefore, the experimental results reported by Dhaiman et al. [6] for rectangular duct parallel pass solar air heater are compared with simulation results on the basis of thermal energy gain and effective efficiency are shown in Fig. 2. The deviation between the experimental and simulation results are calculated by using a Relative percentage error method has been defined as

$$RPE = \frac{|\ddot{X} - \dot{X}|}{\dot{X}} \quad [49]$$

The relative percentage error for thermal energy gain and effective efficiency is about 10.2% and 9.3% respectively. Thus, from the Fig. 2 and RPE values it is observed that the present model has good agreement with experimental results and it is reliable for further analysis of solar air heater.

3.2. Effect of hybrid duct design configuration on thermal performance of SAH

The performance improvement achieved due to utilization of hybrid duct parallel pass smooth plate SAH and hybrid duct parallel pass SAH with inclined ribs are compared with conventional rectangular duct parallel pass SAH is shown in Fig. 3. From the fig, it is observed that the thermal efficiency of all the three SAHs increases with the increase in mass flow rate. Then this value is getting flattened and there is no further appreciable rise in thermal efficiency of SAHs. The fact which influence behavior of SAH is that when increasing the mass flow rate of air increases the flow velocity, heat capacity and heat transfer coefficient between absorber plate and flowing fluid.

The effective efficiency of the SAHs is initially increasing at lower mass flow rates. Then further improvement in mass flow rate reduces the effective efficiency due to increase in pressure drop and pumping power required for propelling the air. The energy balance between the useful thermal energy gain and pumping power consumption by the SAH is shown in the Fig. 4. At higher mass flow rates, there is less appreciable improvement in useful energy gain. At the same time the pumping power consumed by the SAH

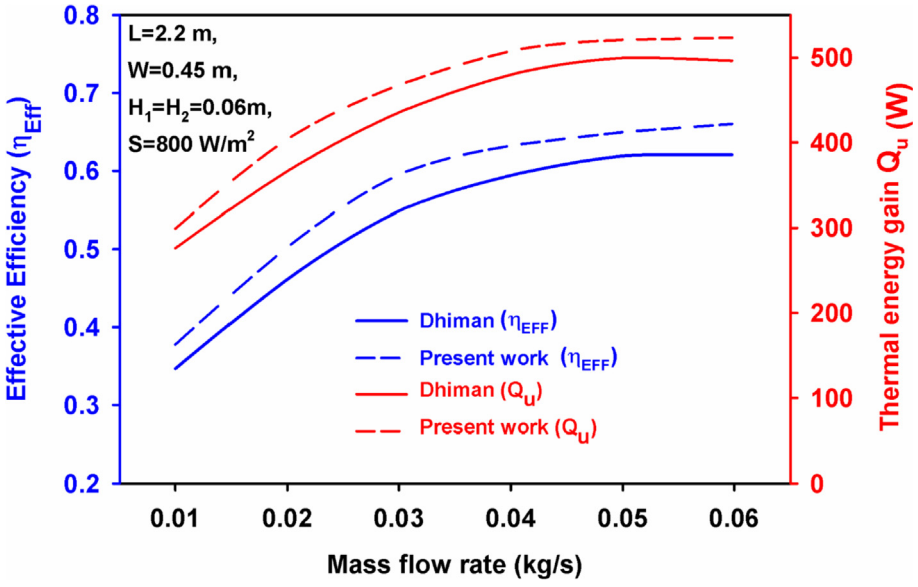

Fig. 2. Validation of analytical model of parallel pass rectangular duct solar air heater.

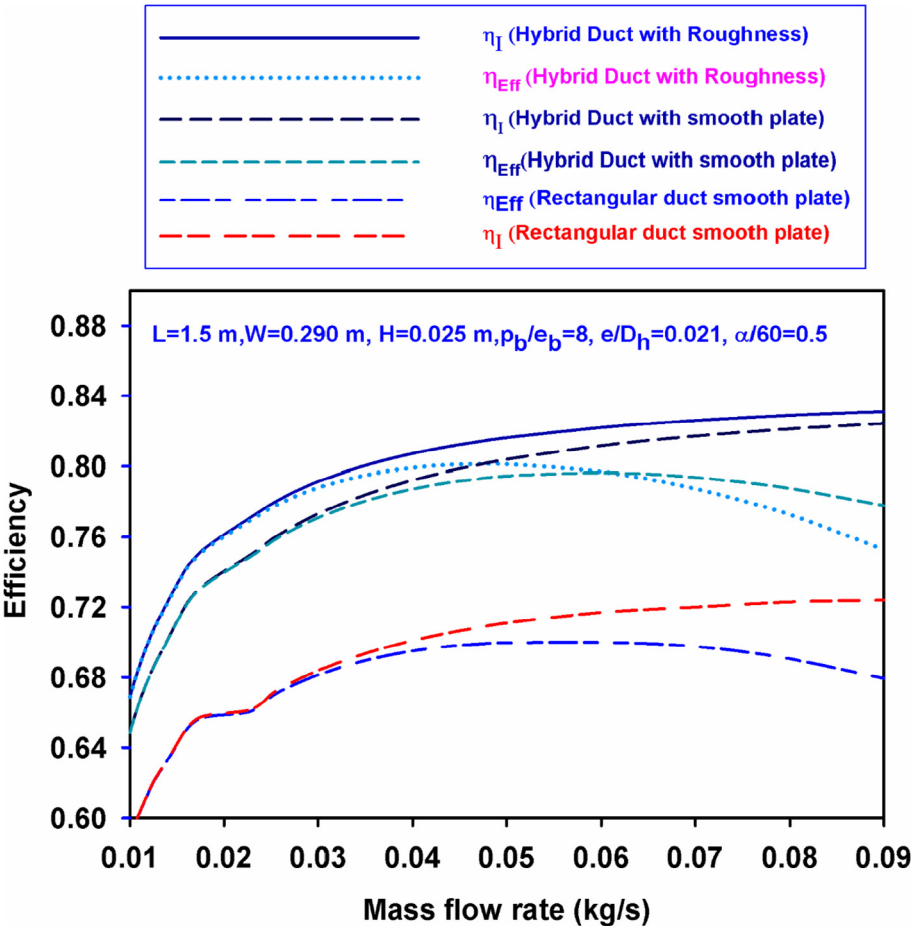

Fig. 3. Thermal performance comparison between solar air heaters.

increases exponentially. At a particular operating condition, the energy converted by the SAH is equal to pumping power and the effective efficiency approaches to zero. The hybrid duct parallel pass smooth plate SAH and hybrid duct parallel pass SAH with inclined ribs are improving the thermal efficiency by 21.3% and 22.4% when compared to conventional rectangular duct parallel pass SAH. It is also improving the effective.

Efficiency by 13.1% and 18.1% respectively. The fact which

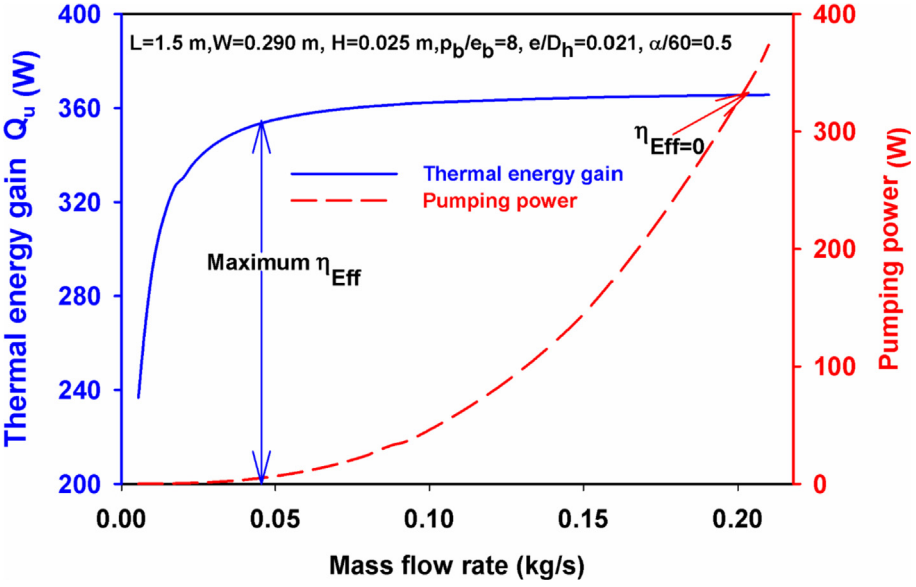

Fig. 4. Influence of mass flow rate on thermal or useful energy gain and pumping power.

influence the improvement of SAH performance is that when using the triangular duct at lower path increases the surface area which enhances the convective heat transfer coefficient. Further attaching the inclined ribs at the top and bottom of the absorber plate breaks the laminar sublayer creation and also enhances the vicinity of reattachment points. Therefore, due to these combined effects improves the rate of heat transfer and enhances the thermal performance of proposed SAH.

3.3. Effect of relative height ratio (e/Dh)

The influence of the relative height ratio (e/Dh) on the effective efficiency of PPHDSAH with inclined ribs is shown in Figs. 5 and 6. The relative height ratio ranges from 0.021 to 0.050. From the Fig. 5 it is revealed that for all the values of relative height ratios the effective efficiency increases and attains its peak value for the critical mass flow rate. The critical values of mass flow rate for each relative height ratios are ranging from 0.0425 to 0.0475 kg/s. Then further increment in mass flow rate leads to declines the thermo hydraulic performance.

From the figure it is also known that the relative height ratio of (e/D_h) 0.050 produces better performance at when the mass flow rate attains up to 0.03 kg/s. This is due to the fact that at lower mass flow rates the higher rib height improves the convective heat transfer rate by breaking the laminar sublayer. Then further increasing the mass flow rate beyond at 0.045 kg/s relative height ratio of (e/D_h) 0.023 accomplishes better performance. This is due to that at higher mass flow rates this higher roughness height offers more resistance and increases the pumping power consumption. Therefore, at higher flow rates lower value of e/D_h yields better performance. The figure also reveals that when mass flow rate increases beyond the value of 0.06 kg/s the PPHDSAH with smooth plate over comes the performance of PPHDSAH with inclined ribs. This happens due to the fact that during this condition the inclined ribs consumes considerable amount of energy for overcome the friction.

Fig. 6 exemplifies the interrelationship among the temperature rise parameter (TRP) ($\Delta T/I$) and thermohydraulic efficiency as a function of the relative height ratio (e/D_h) at constant solar radiation of 1000 W/m^2. From the figure it is detected that when the (TRP) $\Delta T/I < 0.0028$ K m^2/W the PPHDSAH with smooth plate yields highest effective efficiency. Beyond this value once the $\Delta T/I$ is ranges from 0.0028 to 0.0035 K m^2/W the e/D_h of 0.023 produces maximum performance when compared with other values. Further,

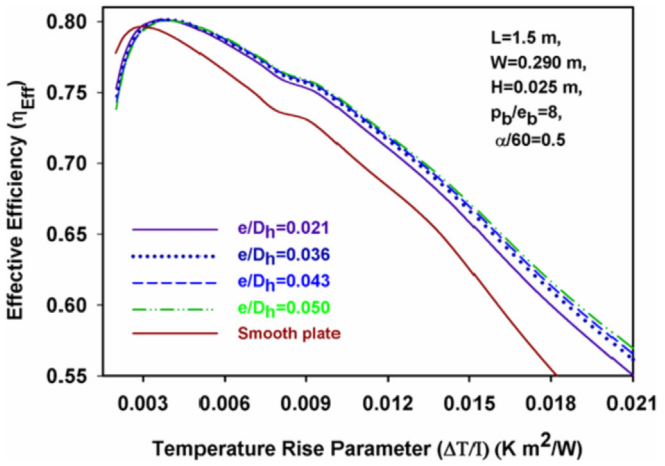

Fig. 6. Effective efficiency as a function of Temperature rise parameter and relative roughness height (e/D_h).

when the $\Delta T/I > 0.0049$ K m^2/W the e/D_h value of 0.05 have produced better performance.

3.4. Effect of relative angle of attack (α/60)

The effective efficiency of PPHDSAH with inclined ribs varies with respect to mass flow rate, Temperature rise parameter and relative angle of attack are presented in Figs. 7 and 8. During the analysis the relative angle of attack ranges from 0.5 to 1 and all other roughness parameters are remaining constant. The higher value of effective efficiency is found for relative angle of attack (α/60) of 1 for the rate of air flow less than 0.0325 kg/s. Further increment in flow rate of air yields the highest effective efficiency for the relative angle of attack (α/60) of 0.5. This happens due to that during lower air flow rates higher inclination angle generates more secondary flow separation and during the reattachment with a primary flow which improves the heat transfer rate. While increasing the mass flow rate this behavior is reversed and the lower value of α/60 creates more secondary flow. For all the values of the relative angle of attack considered in this analysis follows the similar trend. That is initially the thermal performance is increased and reaches its peak value, then it follows a declining trend at further increment in mass flow rate. The overall maximum

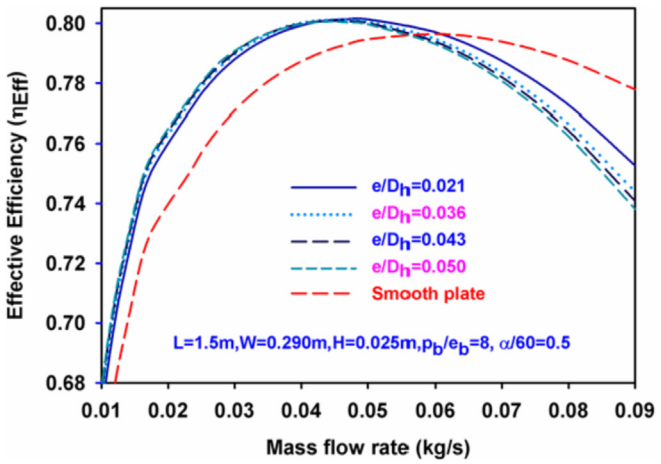

Fig. 5. Effective efficiency as a function of mass flow rate and relative roughness height (e/D_h).

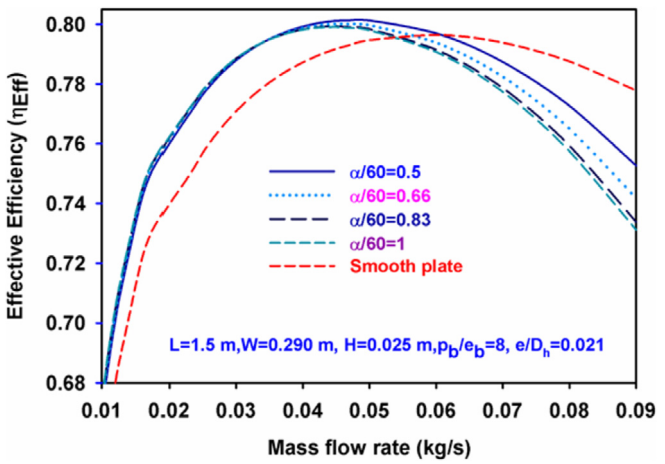

Fig. 7. Effective efficiency as a function of mass flow rate and relative angle of arc (α/60).

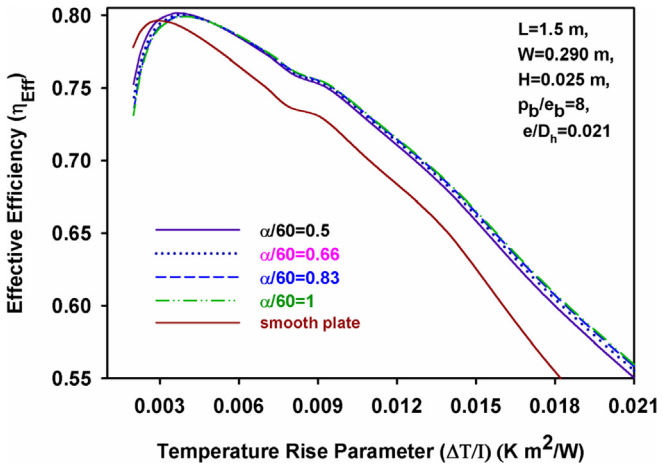

Fig. 8. Effective efficiency as a function of Temperature rise parameter and relative angle of arc (α/60).

performance is given by the relative angle of attack (α/60) of 0.5.

Fig. 8 also shows the identical trend, that the effective efficiency increases with an increase in the temperature rise parameter (ΔT/I) then it starts to decrease after attains its maximum value. The PPHDSAH with smooth plate yields maximum efficiency at when the (TRP) ΔT/I < 0.0028 K m^2/W. Then a further raise in the TRP the relative angle of attack (α/60) of 0.5 have performed better up to 0.00410 K m^2/W.Beyond this range of temperature rise parameter (ΔT/I) the relative angle of attack (α/60) of 1 have dominant performance when compared with other values.

3.5. Effect of relative roughness pitch (P_b/e_b)

Fig. 9 shows the relation between the mass flow rate and effective efficiency as a function of relative roughness pitch (P_b/e_b) at the bottom side of the absorber plate. Throughout the analysis the relative roughness pitch at the top of the absorber plate is equal to 10 and at bottom it ranges from 4 to 16. The relative roughness pitch (P_b/e_b) of 8 produces the maximum effective efficiency when compared with other values over the entire range of mass flow rate are considered. When the relative roughness pitch (P_b/e_b) increases from 4 to 8 the effective efficiency is increased. Then a further increase in relative roughness pitch (Pb/e_b) reduces the thermal performance.

This happens due to the fact that at lower values of roughness pitch increases the number of roughness surfaces that improves the heat transfer. But it also consumes the higher pumping power to overcome the friction occurs inside the duct. Therefore, the effective efficiency is decreased. During at higher values of roughness pitch, decreases the number of roughness surfaces which degraded the secondary flow separation and reattachment. Therefore, at P_b/e_b value of 8 having optimum performance with better enhancements in heat transfer with reasonable consumption of pumping power.

The variation of relative roughness pitch (P_b/e_b) on the effective efficiency as a function of temperature rise parameter (TRP) (ΔT/I) is shown in Fig. 10. When the TRP-ΔT/I < 0.0028 K m^2/W PPHDSAH with smooth plate performs better beyond this value the relative roughness pitch (P_b/e_b) of 8 yields maximum performance over the entire range of operating conditions.

3.6. Effect of mass flow fraction on effective efficiency (i)

The variation of effective efficiency of PPHDSAH with mass flow fraction at various values of total mass flow rate (G) is shown in Fig. 11. The mass flow fraction is defined as the ratio between the amount of airflow at upper rectangular duct to total mass flow rate. The figure shows that when increasing the total mass flow rate the effective efficiency also increased for all the values of mass flow fractions (i) considered in this analysis. At lower mass flow rates (m < 0.035 kg/s) the 'i' value of 0.9 yields dominant performance. For higher values (m > 0.04 kg/s) the 'i' value shifted to 0.5.

The maximum value of effective efficiency increases gradually when increasing the value of the mass flow fraction (i) up to 0.5. Then a further increase in the mass flow fraction (i) decreases the performance. Therefore, the optimum value of i = 0.5 with maximum effective efficiency of 80.12%. This happens due to the fact that at when the flow is equal on both the sides of the absorber plate, the PPHDSAH enhances the heat transfer and also consumes less pumping power. If flow rate is higher at upper side it improves the heat transfer with the penalty of pumping power. In the same way that the air flow at lower duct is increased which reduces the pumping power and also reduction in heat transfer. Therefore, both the conditions lead through decreases the effective efficiency.

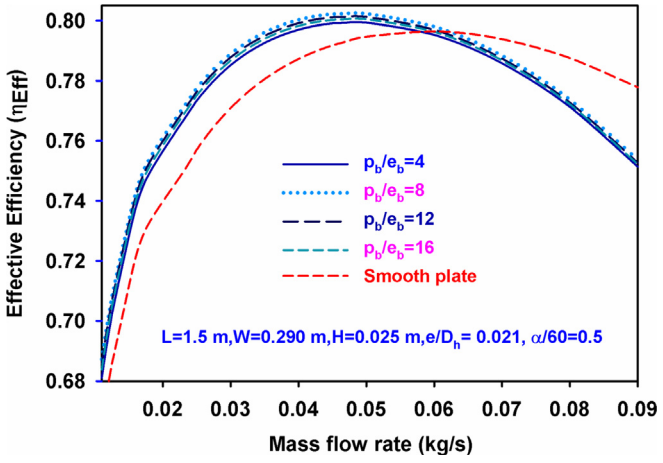

Fig. 9. Effective efficiency as a function of mass flow rate and relative roughness pitch (p_b/e_b).

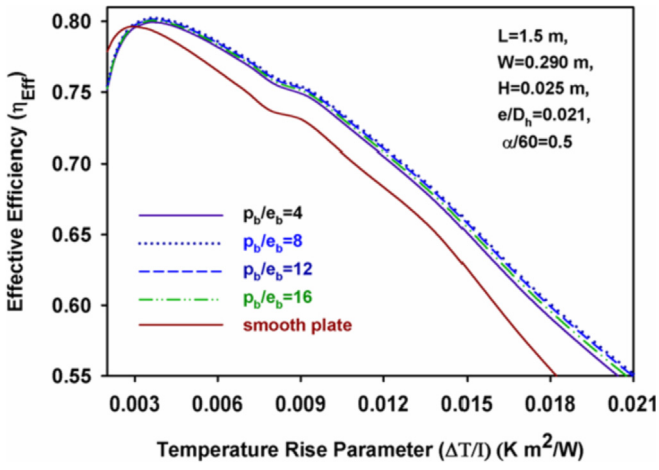

Fig. 10. Effective efficiency as a function of Temperature rise parameter and relative roughness pitch (p_b/e_b)).

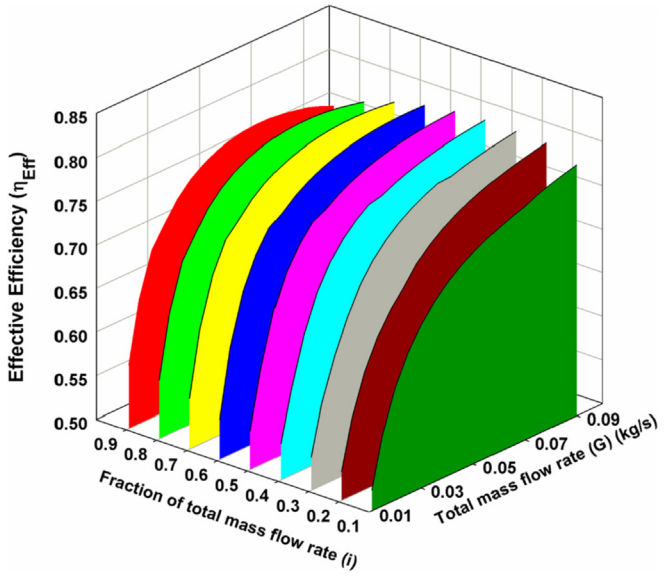

Fig. 11. Effective efficiency as a function of total mass flow rate and mass flow fraction (i).

3.7. Thermal performance comparison between proposed SAH with literature

The thermal performance of the proposed solar air heater is compared with experimental values obtained for parallel pass and packed bed parallel pass SAHs analyzed by Dhaiman et al. [6]. Fig. 12 shows the comparison which is carried out in similar operating conditions with identical collector dimensions.

The comparison result clearly shows that the PPHDSAH have better performance at all the flow rates, which is considered in the analysis. It improves the effective efficiency by 16.2% and 14.3% when compared to parallel pass and packed bed parallel pass SAH respectively.

3.7.1. Design plots for optimizing the roughness parameters

To evaluate the optimum values of PPHDSAH roughness parameters based on the highest values of effective efficiency the design plots are shown in Figs. 13–14. The design plots are plotted as a function of the temperature rise parameter. The variation of the relative roughness height ratio (e/D_h) for three different solar isolations of 500 W/m^2, 750 W/m^2 and 1000 W/m^2 is shown in Fig. 13. The figure exemplifies that when the temperature rise parameter is < 0.0038 K m^2/W, relative roughness height ratio (e/D_h) of 0.021 yields an optimum value and the value shift to 0.050 when the TRP ($\Delta T/I$) > 0.005 K m^2/W. When the TRP is in between in the rage of 0.0038–0.005 K m^2/W various values of the relative roughness height ratio (e/D_h) provide optimum value and this value follows an increasing trend when the solar radiation is increased.

In the same manner the design plot for relative angle of attack ($\alpha/60$) as a function of solar radiation is shown in Fig. 14.

The optimum value of the relative angle of attack ($\alpha/60$) is 0.5 for the temperature rise parameter lesser than 0.0039 K m^2/W and 1 for $\Delta T/I$ > 0.0049 K m^2/W. The temperature rise parameters are in between 0.0039 and 0.0049 K m^2/W the optimum values are as a function of solar insolation (I). From the Fig. 10 it is known that the optimum value of the relative pitch ratio is (P/e) 8 for all the operating conditions. Therefore, the separate design plot is not essential for expressing this optimized value.

4. Conclusion

In this work, the mathematical model for parallel pass hybrid duct solar air heater with inclined ribs is developed and its thermal performance is evaluated. Based on the previous results and discussions the following conclusions are summarized as.

- The parallel pass hybrid duct solar air heater with inclined ribs enhances the thermal and effective efficiency by 22.4% and 18.1% when compared to conventional rectangular duct parallel pass SAH.
- With the increase in mass flow rate enhances the effective efficiency and reaches its maximum value, then follows a decreasing trend with further increase in mass flow rate. Based on the effective efficiency it is concluded that the parallel pass hybrid duct solar air heater with inclined ribs is suitable to operate up to the mass flow rate of 0.06 kg/s. Over the range of mass flow rate the parallel pass hybrid duct solar air heater with smooth plate performs better.
- During this analysis, it is identified that the optimum values of roughness parameters are relative roughness height (e/D_h) of 0.021, relative roughness pitch (Pb/e_b) of 8 and relative angle of arc ($\alpha/60$) of 0.5 which yields the maximum effective efficiency of 80.12%.
- The effect of the mass flow ratio (i) on the thermal performance of the proposed solar air heater is evaluated and it is found that

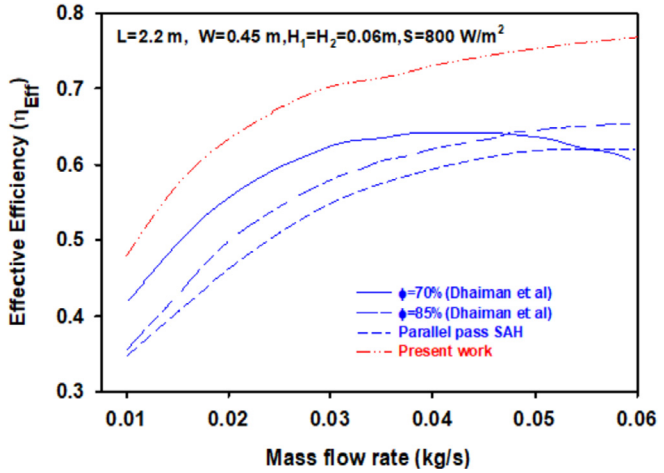

Fig. 12. Thermal performance-based comparison between PPHDSAH with roughness against SAH available in literature [6].

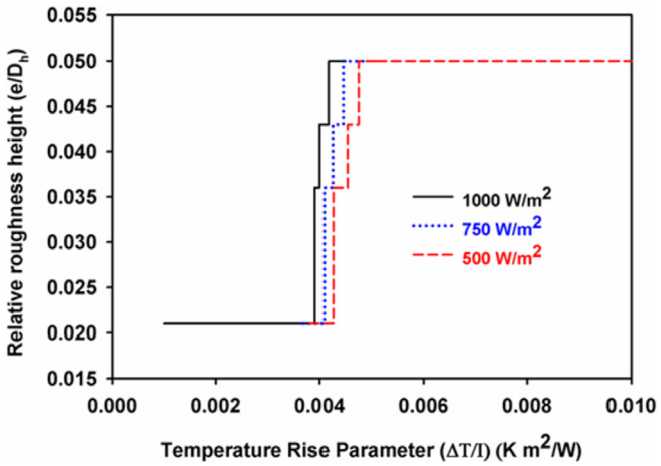

Fig. 13. Optimum value of relative roughness height at different values of insolation and temperature rise parameter.

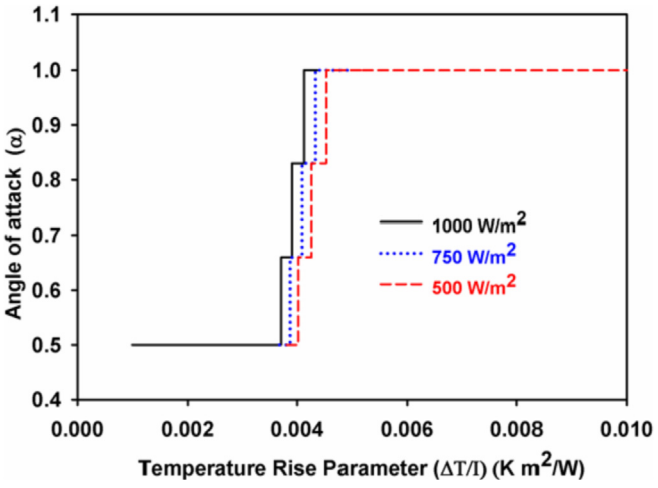

Fig. 14. Optimum value of angle of arc at different values of insolation and temperature rise parameter.

when the i = 0.5 the maximum value of effective efficiency is achieved.

- The design plots are prepared and intended for identifying the optimal configurations of roughness parameters of SAH, which yields the maximum effective efficiency with required temperature rise parameter.

Declaration of competing interest

The authors declare that they have no known competing financial interests or personal relationships that could have appeared to influence the work reported in this paper.

References

[1] S. Singh, P. Dhiman, Thermal performance of double pass packed bed solar air heaters - a comprehensive review, Renew. Sustain. Energy Rev. 53 (2016) 1010–1031, https://doi.org/10.1016/j.rser.2015.09.058.

[2] H. Yeh, C. Ho, J. Hou, The improvement of collector efficiency in solar air heaters by simultaneously air flow over and under the absorbing plate, Energy 24 (1999) 857–871, https://doi.org/10.1016/S0360-5442(99)00043-2.

[3] M.R.I. Ramadan, S.M. Shalaby, S. Aboul-Enein, B.M. Moharram, A.A. El-Sebaii, Investigation of thermal performance of-double pass-flat and v-corrugated plate solar air heaters, Energy 36 (2011) 1076–1086, https://doi.org/10.1016/j.energy.2010.11.042.

[4] S. Rai, P. Chand, S.P. Sharma, Evaluation of thermo hydraulic effect on offset finned absorber solar air heater, Renew. Energy 125 (2018) 39–54, https://doi.org/10.1016/j.renene.2018.01.110.

[5] P. Dhiman, N.S. Thakur, S.R. Chauhan, Thermal and thermohydraulic performance of counter and parallel flow packed bed solar air heaters, Renew. Energy 46 (2012) 259–268, https://doi.org/10.1016/j.renene.2012.03.032.

[6] P. Dhiman, N.S. Thakur, A. Kumar, S. Singh, An analytical model to predict the thermal performance of a novel parallel flow packed bed solar air heater, Appl. Energy 88 (2011) 2157–2167, https://doi.org/10.1016/j.apenergy.2010.12.033.

[7] M.M. Matheswaran, T.V. Arjunan, D. Somasundaram, Analytical investigation of solar air heater with jet impingement using energy and exergy analysis, Sol. Energy 161 (2018) 25–37, https://doi.org/10.1016/j.solener.2017.12.036.

[8] M.M. Matheswaran, T.V. Arjunan, D. Somasundaram, Energetic, exergetic and enviro-economic analysis of parallel pass jet plate solar air heater with artificial roughness, J. Therm. Anal. Calorim. (2018), https://doi.org/10.1007/s10973-018-7727-4.

[9] V. Singh Bisht, A. Kumar Patil, A. Gupta, Review and performance evaluation of roughened solar air heaters, Renew. Sustain. Energy Rev. 81 (2018) 954–977, https://doi.org/10.1016/j.rser.2017.08.036.

[10] D. Gupta, S.C. Solanki, J.S. Saini, Thermohydraulic performance of solar air heaters with roughened absorber plates, Sol. Energy 61 (1997) 33–42, https://doi.org/10.1016/S0038-092X(97)00005-4.

[11] R. Karwa, K. Chauhan, Performance evaluation of solar air heaters having v-down discrete rib roughness on the absorber plate, Energy 35 (2009) 398–409, https://doi.org/10.1016/j.energy.2009.10.007.

[12] R. Karwa, G. Chitoshiya, Performance study of solar air heater having v-down discrete ribs on absorber plate, Energy 55 (2013) 939–955, https://doi.org/10.1016/j.energy.2013.03.068.

[13] V.B. Gawande, A.S. Dhoble, D.B. Zodpe, S. Chamoli, Analytical approach for evaluation of thermo hydraulic performance of roughened solar air heater, Case Stud. Therm. Eng. 8 (2016) 19–31, https://doi.org/10.1016/j.csite.2016.03.003.

[14] B. Bhushan, R. Singh, Thermal and thermohydraulic performance of roughened solar air heater having protruded absorber plate, Sol. Energy 86 (2012) 3388–3396, https://doi.org/10.1016/j.solener.2012.09.004.

[15] M.K. Sahu, R.K. Prasad, Thermohydraulic performance analysis of an arc shape wire roughened solar air heater, Renew. Energy 108 (2017) 598–614, https://doi.org/10.1016/j.renene.2017.02.075.

[16] D.S. Thakur, M.K. Khan, M. Pathak, Performance evaluation of solar air heater with novel hyperbolic rib geometry, Renew. Energy 105 (2017) 786–797, https://doi.org/10.1016/j.renene.2016.12.092.

[17] V. Kumar, Nusselt number and friction factor correlations of three sides concave dimple roughened solar air heater, Renew. Energy 135 (2019) 355–377, https://doi.org/10.1016/j.renene.2018.12.002.

[18] A. Kumar, A. Layek, Nusselt number and friction factor correlation of solar air heater having twisted-rib roughness on absorber plate, Renew. Energy 130 (2019) 687–699, https://doi.org/10.1016/j.renene.2018.06.076.

[19] A. Kumar, A. Layek, Thermo-hydraulic performance of solar air heater having twisted rib over the absorber plate, Int. J. Therm. Sci. 133 (2018) 181–195, https://doi.org/10.1016/j.ijthermalsci.2018.07.026.

[20] I. Singh, S. Singh, CFD analysis of solar air heater duct having square wave profiled transverse ribs as roughness elements, Sol. Energy 162 (2018) 442–453, https://doi.org/10.1016/j.solener.2018.01.019.

[21] P.K. Jain, A. Lanjewar, Overview of V-RIB geometries in solar air heater and performance evaluation of a new V-RIB geometry, Renew. Energy 133 (2019) 77–90, https://doi.org/10.1016/j.renene.2018.10.001.

[22] M.G. Gabhane, A.B. Kanase-Patil, Experimental analysis of double flow solar air heater with multiple C shape roughness, Sol. Energy 155 (2017) 1411–1416, https://doi.org/10.1016/j.solener.2017.07.038.

[23] R. Kumar, A. Kumar, Thermal and fluid dynamic characteristics of flow through triangular cross-sectional duct : a review, Renew. Sustain. Energy Rev. 61 (2016) 123–140, https://doi.org/10.1016/j.rser.2016.03.011.

[24] V. Goel, P. Guleria, R. Kumar, Effect of apex angle variation on thermal and hydraulic performance of roughened triangular duct, Int. Commun. Heat Mass Transf. 86 (2017) 239–244, https://doi.org/10.1016/j.icheatmasstransfer.2017.06.008.

[25] R. Kumar, S. Khurana, A. Kumar, V. Goel, Effect of dimple intrusions and curvature radius of rounded corner triangular duct on fluid flow and heat transfer, J. Therm. Sci. Eng. Appl. 11 (2018), 031001, https://doi.org/10.1115/1.4041683.

[26] R. Kumar, Varun, A. Kumar, Experimental and computational fluid dynamics study on fluid flow and heat transfer in triangular passage solar air heater of different configurations, J. Sol. Energy Eng. 139 (2017), 041013, https://doi.org/10.1115/1.4036775.

[27] R. Kumar, A. Kumar, V. Goel, Effect of rounded corners on heat transfer and fluid flow through triangular duct, J. Heat Transf. 140 (2018) 121701, https://doi.org/10.1115/1.4040957.

[28] V. Goel, A. Kumar, S.B. Bopche, R. Kumar, S. Khurana, P. Singh, Numerical investigation of heat transfer and friction factor in ribbed triangular duct solar air heater using Computational fluid dynamics (CFD), J. Mech. Sci. Technol. 32 (2018) 399–404, https://doi.org/10.1007/s12206-017-1240-8.

[29] R. Kumar, V. Goel, A. Kumar, Investigation of heat transfer augmentation and friction factor in triangular duct solar air heater due to forward facing chamfered rectangular ribs: a CFD based analysis, Renew. Energy 115 (2018) 824–835, https://doi.org/10.1016/j.renene.2017.09.010.

[30] R. Kumar, A. Kumar, V. Goel, Performance improvement and development of correlation for friction factor and heat transfer using computational fluid dynamics for ribbed triangular duct solar air heater, Renew. Energy 131 (2019) 788–799, https://doi.org/10.1016/j.renene.2018.07.078.

[31] G. Bharadwaj, R. Kumar Varun, A. Sharma, Heat transfer augmentation and flow characteristics in ribbed triangular duct solar air heater: an experimental analysis, Int. J. Green Energy 14 (2017) 587–598, https://doi.org/10.1080/15435075.2017.1307751.

[32] M.M. Matheswaran, T.V. Arjunan, D. Somasundaram, Energetic, exergetic and enviro-economic analysis of parallel pass jet plate solar air heater with artificial roughness, J. Therm. Anal. Calorim. (2018), https://doi.org/10.1007/s10973-018-7727-4.

[33] K. Mohammadi, M. Sabzpooshani, Appraising the performance of a baffled solar air heater with external recycle, Energy Convers. Manag. 88 (2014) 239–250, https://doi.org/10.1016/j.enconman.2014.08.009.

[34] A. Fudholi, K. Sopian, M.H. Ruslan, M.Y. Othman, Performance and cost benefits analysis of double-pass solar collector with and without fins, Energy Convers. Manag. 76 (2013) 8–19, https://doi.org/10.1016/j.enconman.2013.07.015.

[35] K.S. Ong, Thermal performance of solar air heaters: mathematical model and solution procedure, Sol. Energy 55 (1995) 93–109, https://doi.org/10.1016/00380-92X9(50)0021I-.

[36] J.A. Duffie, W.A. Beckman, Solar Engineering of Thermal Processes, fourth ed., 2013, https://doi.org/10.1002/9781118671603.

[37] P.T. Saravanakumar, D. Somasundaram, M.M. Matheswaran, Thermal and thermo-hydraulic analysis of arc shaped rib roughened solar air heater integrated with fins and baffles, Sol. Energy 180 (2019) 360–371, https://doi.org/10.1016/j.solener.2019.01.036.